Title
Swelling of individual nanodomains in hydrated block copolymer electrolyte membranes

Journal
The Journal of Chemical Physics, 149(16)

ISSN
0021-9606

Authors
Chen, X Chelsea
Jiang, Xi
Balsara, Nitash P

Publication Date
2018-10-28

DOI
10.1063/1.5029452

Peer reviewed

Swelling of Individual Nanodomains in Hydrated Block Copolymer Electrolyte Membranes

X. Chelsea Chen[a], Xi Jiang[a], and Nitash P. Balsara[a,b,c]

[a]Materials Sciences Division, Lawrence Berkeley National Laboratory, Berkeley, CA 94720

[b]Department of Chemical and Biomolecular Engineering, University of California, Berkeley, CA 94720

[c]Energy Technologies Area, Lawrence Berkeley National Laboratory, Berkeley, CA 94720

Abstract

In this work, we examine the swelling of nanostructured block copolymer electrolytes immersed in liquid water. A series of sulfonated polystyrene-*b*-polyethylene-*b*-polystyrene (S-SES) membranes having the same nominal chemical composition but two different morphologies are prepared by systematic changes in processing. We start with a membrane comprising a mixture of homopolymer polystyrene (hPS) and a polystyrene-*b*-polyethylene-*b*-polystyrene (SES) copolymer. Homopolymer hPS is subsequently selectively removed from the membrane and the polystyrene domains are sulfonated to give S-SES membranes. The morphology of the membranes is controlled by controlling ϕ_v, the volume fraction of hPS in the blended membrane. The morphology of the membranes was studied by small angle X-ray scattering (SAXS), cryogenic scanning transmission electron microscopy (cryo-STEM) and cryogenic electron tomography. The overall domain swelling measured by SAXS decreases slightly at ϕ_v =0.29; a cross-over from lamellar to bicontinuous morphology is obtained at the same value of ϕ_v. The bicontinuous morphologies absorb more water than the lamellar morphologies. In contrast, the nanodomain swelling of the bicontinuous membrane (120%) is slightly less than that of the lamellar

membrane (150%). Quantitative analysis of the STEM images and electron tomography was used determine the swelling on the hydrophilic and hydrophobic domains due to exposure to water. The hydrophilic PSS-rich domain spacing increases while the hydrophobic PE domain spacing decreases when the membranes are hydrated. The extent of increase and decrease is not a strong function of ϕ_v.

Introduction

Polymer electrolyte membranes have attracted considerable attention due to their wide applications in fuel cells,[1, 2] redox flow cells,[3, 4] lithium batteries[5, 6] and clean water technologies such as electrodialysis.[7, 8] Ion transport in polymer electrolyte membranes are often facilitated by the presence of solvents like water,[9-11] methanol[12, 13] and ionic liquid.[14, 15] Swelling of polymer electrolyte membranes by such solvents is an important issue as it affects the concentration of ionic groups in the swollen membrane hence the ion transport rate. Swelling also affects the mechanical properties and dimensional stability of the membranes, both having impact on the performance of the device. The macroscopic swelling of polymer electrolyte membranes in water has been studied extensively.[10, 16, 17] However, there have been very few studies probing the swelling (or deswelling) of individual nanodomains in polymer electrolyte membranes.[18, 19] While one expects the

hydrophilic domains to swell in the hydrated, predicting the concomitant changes in the size of the hydrophobic domains is more challenging.

Block copolymer electrolytes consisting of a hydrophobic structural block and a hydrophilic ion transporting block serve as a good model platform to study the nanoscale swelling of such membranes in the presence of solvents.[20, 21] Block copolymers can self-assemble into a variety of well-defined morphologies, depending on the volume fraction of the two blocks. Swelling one block with a selective solvent may change the phase behavior of the block copolymer as it changes the effective Flory-Huggins parameter χ between the two blocks.[22, 23] When one of the blocks is charged, the phase behavior of block copolymer electrolyte/solvent mixture becomes more complicated.

In previous reports, we examined the effects of molecular weight, composition, and sulfonation level on the phase behavior of block copolymer electrolyte poly(styrene sulfonate methylbutylene) (PSS-PMB).[21, 24, 25] We found that in the dry state, PSS-PMB exhibited rich morphologies at regimes where uncharged block copolymers only exhibit lamellar morphology. PSS-PMB with a very low molecular weight ($M_{n,PS}$ =1.4 kg/mol and $M_{n,PMB}$ =1.4 kg/mol, sulfonation level = 30%) exhibited a disorder-to-order transition with increasing temperature at fixed relative humidity above 54%, while PSS-PMB with a higher molecular weight and lower sulfonation level ($M_{n,PS}$ =2.5 kg/mol and $M_{n,PMB}$ =2.6 kg/mol, sulfonation level = 9%) exhibited a lamellar-to-disorder transition with increasing temperature at a fixed relative humidity of

85%. These transitions were driven by the partial molar entropy change of water, which can be determined directly by measuring the order-to-disorder transition temperature of the hydrated membrane in equilibrium with humid air. It is worth nothing that water uptake did not show a discontinuous change at these transitions.

Recently, we explored the effect of hydration on a sulfonated polystyrene-*b*-polyethylene-*b*-polystyrene (S-SES) triblock copolymer. We reported direct observation of water-rich channels in S-SES membranes equilibrated in liquid water.[26] The presence of these channels coincides with a sharp discontinuous increase in proton conductivity of the membranes when the environment transitioned from nearly saturated humid air to liquid water. Furthermore, we discovered that the introduction of pores into block copolymer membranes prior to sulfonation provided additional control over water uptake and conductivity.[27] The fabrication and characterization of the porous membranes are discussed in ref 27.

The focus of this work is to study and understand the nanoscale swelling behavior of S-SES membranes. We fabricated a series of non-porous and porous S-SES membranes with the same nominal composition but with varying morphologies. We demonstrate that when S-SES membranes absorb water from a liquid water reservoir, the sulfonated polystyrene (PSS) block swells extensively, and no order-to-order transition was observed. The nanodomain swelling within these membranes was examined by small angle X-ray scattering (SAXS), cryogenic scanning

transmission electron microscopy (cryo-STEM) and cryogenic electron tomography. This paper is part of the series on the interplay between morphology, solvent uptake and ion transport through block copolymer electrolyte membranes.[21, 24-29]

Experimental

Materials: Homopolymer polystyrene (hPS) and polystyrene-*b*-polyethylene-*b*-polystyrene (SES) triblock copolymer was synthesized using anionic polymerization protocol described in Ref 26.[26] The molecular weight of hPS used in this work was 5.9 kg/mol, with a dispersity of 1.06. The molecular weights of polystyrene (PS) and polyethylene (PE) blocks of SES were 13.8 and 18.7 kg/mol, respectively.

Membrane fabrication: Predetermined ratios of hPS and SES were dissolved in *o*-xylene and gently stirred at 100 °C for 4 hours. The solution was then cast on an ultraclean aluminum foil using a custom-built solvent caster equipped with a doctor blade at 80 °C. The concentration of the solution and the height of the doctor blade were adjusted to obtain membranes with thicknesses of 40 ± 5 μm. The membranes were dried under vacuum at 80 °C for 24 hours. After drying, the aluminum foil was removed by immersing the membrane (with the aluminum foil stuck to it) in 1M hydrochloric acid. The resulting free-standing membrane was washed with deionized water several times and dried under vacuum for 16 hours.

The hPS/SES blend membranes were washed with THF at room temperature, to selectively dissolve hPS, followed by a methanol rinse. This is repeated three times to ensure complete removal of hPS. The weight of the membranes before and after washing was measured. For all the membranes used in the study, the weight of hPS originally blended into SES was equal to the weight extracted. We define the nominal void volume fraction, ϕ_v, as the volume fraction of hPS that was blended with SES and subsequently extracted.

Pristine nonporous SES membranes were prepared following the same steps described above for systematic comparison (acid wash followed by THF/methanol rinses).

SES membranes (porous and nonporous) were sulfonated in a custom-designed three-neck reactor. A membrane with 2 inch diameter was punched out and held in place with a custom-designed Teflon clamp inside the reactor. The sulfonation reaction was conducted in 1,2-dibloroethane with acetic sulfate as the sulfonating agent, as reported previously. The sulfonated membranes (S-SES) were stored in deionized water prior to measurements.

Determination of Ion Content: Ion exchange capacity (*IEC*), defined as the milliequivalents of sulfonic acid groups per dry gram of polymer (mmol/g), was measured using the following procedure[16]: a piece of water-equilibrated membrane was immersed in 1M NaCl, and gently stirred for 16

hours. During this time, the H^+ ions in the membrane are replaced by Na^+ ions. After completion of ion exchange, membrane was removed from the solution. The solution was titrated with a standard 0.01M NaOH solution to the phenolphthalein endpoint. The membrane was then soaked in 0.1 M HCl for 2 hours to return it to the acid form. After acid treatment, the membrane was washed with deionized water several times and soaked in deionized water for 16 hours. Finally the membrane was dried under vacuum at room temperature for 24 hours and then at 80 °C for two hours. It was allowed to cool down in a desiccator before the dry weight, W_{dry}, was measured. *IEC* is calculated using equation 1.

$$IEC\,(mmol/g) = \frac{\text{volume of NaOH solution}\,(\text{mL}) \times \text{concentration of NaOH solution (M)}}{\text{W}_{\text{dry}}\ (\text{g})} \quad (1)$$

The sulfonation level (*SL*) of S-SES, defined by equation 2, was calculated from *IEC* and the weight fraction of PS block in SES.

$$SL = \frac{mol\,SSA}{mol\,S + mol\,SSA} \quad (2)$$

where SSA is styrene sulfonic acid and S is styrene.

Water uptake: Water uptake, *WU*, of the membranes is defined by equation 3,

$$WU = \frac{W_{wet} - W_{dry}}{W_{dry}} \times 100\% \quad (3)$$

where W_{wet} is the wet weight of the membrane and W_{dry} is the dry weight of the membrane. To obtain W_{wet}, a piece of water-equilibrated membrane was taken out of water and gently dabbed with Kimwipe to remove surface water. The weight of the membrane was then quickly measured on a balance. The hydrated membrane was kept in water for at least 5 days prior to this measurement.[26] Membrane was subsequently dried in vacuum at room temperature for 24 hours and then at 80 °C for two hours. It was allowed to cool down in a desiccator before W_{dry} was measured.

SAXS: Hydrated samples were prepared by sealing a small piece of hydrated membrane in a Teflon washer. The Teflon washer was sandwiched between two pieces of Kapton films and filled with deionized water before sealing with heat resistant sealant. Dry samples were prepared in the same way with no water in the cell. SAXS experiments were performed at beamline 7.3.3 at the Advanced Light Source (ALS) at Lawrence Berkeley National Laboratory (LBNL) as well as beamline 1-5 at the Stanford Synchrotron Radiation Lightsource (SSRL) at SLAC National Accelerator Laboratory. The original two-dimensional scattering images were azimuthally averaged to generate one-dimensional scattering intensity profiles, *I(q)*. The scattering wave vector $q=4\pi \sin(\theta/2)/\lambda$, where θ is scattering angle and λ is the wavelength of the incident beam. The intensity profile of each dry/hydrated membrane was normalized by their respective transmission coefficients. The scattering profile of an empty sample cell with the same geometry containing the

same amount of water (or no water) was normalized by its own transmission and subtracted from the scattering profile of each membrane.

Cryo-STEM and cryogenic electron tomography: To prepare dry STEM samples, thin sections with thickness about 70 nm were obtained by cryomicrotoming dry S-SES membranes at −140 °C using a Leica EM FC6 cryomicrotome. The thin sections were placed onto a lacey carbon supported copper grid (Electron Microscopy Sciences). Hydrated samples were obtained by annealing the microtomed thin sections in 6 µL of deionized water for 15 min, dabbing off surface water with filter paper and plunging into liquid ethane using an FEI vitrobot (Mark IV). Dark field STEM images were acquired on a Tecnai F20 UT FEG using a high angle annular dark field (HAADF) detector with 200 keV acceleration voltage. Dry samples were imaged at room temperature. Hydrated samples were imaged at −184 °C, using a Gatan 914 high tilt cryo-stage.

For TEM tomography, gold nanoparticles with 10 nm diameter were deposited on the sample to facilitate alignment of the tilt series images. Tomography experiments were performed on a JEOL 3100 microscope using 300 keV acceleration voltage. Single tilt series images were collected in the angle range −65° - 65° for each tilt series. Alignment and reconstruction were done using the IMOD tomographic reconstruction software package. The reconstructed tomogram was segmented and colored using Avizo Standard.

Results and Discussion

We prepared a series of S-SES membranes using the following protocol: we started with a membrane comprising a mixture of homopolymer polystyrene (hPS) and an unsulfonated polystyrene-*b*-polyethylene-*b*-polystyrene (SES) triblock copolymer. Homopolymer polystyrene is selectively removed from the blend membrane, leaving behind a porous SES membrane (for details see the Experimental section). The porosity of the SES membrane, ϕ_v, is assumed to be equal to the volume fraction of hPS in the blend membrane. The porous SES membrane was then sulfonated to produce an S-SES membrane with hydrophilic PSS domains and hydrophobic PE domains. Using this method, we obtained a series of S-SES membranes that have the same nominal chemical composition, differing only slightly in sulfonation levels. In a previous study we examined the pore structure of membranes fabricated following the same protocol.[27] We found that mesoscopic pores are present in the SES membranes prior to sulfonation, but they are not present in the sulfonated S-SES membranes. The membranes used in this work are described in Table 1. We refer to the sulfonated membranes as S-SES(x), where x is the volume percent of hPS that was blended with SES and subsequently extracted.

Table 1 Membranes used in this work.

Sample code	ϕ_v*	***SL* (%)**
S-SES(0)	0	68.3 ± 2.7
S-SES(10)	0.096	63.6 ±

		2.8
S-SES(20)	0.19	59.2 ± 0.4
S-SES(30)	0.29	68.6 ± 2.3
S-SES(40)	0.39	61.4 ± 0.8

*ϕ_v is equal to volume fraction of hPS that was blended with SES and subsequently extracted.

Figure 1 shows the water uptake, *WU*, of S-SES membranes as a function of ϕ_v. Water uptake for these S-SES membranes increased with increasing ϕ_v, from 160% of S-SES(0) to 370% of S-SES(40). This result is consistent with our previous findings.[27, 30]

In order to study the nanodomain swelling of S-SES membranes, we examined their morphologies in both the dry state and in the hydrated state equilibrated in a water reservoir. Figure 2 shows SAXS results on S-SES membranes in the dry state. The profiles are vertically shifted for clarity. All five membranes of interest showed a single broad peak. We fitted each peak with a Lorentzian distribution function provided by the Multi-peak Fit Package of Igor Pro 6.37. Typical peak fitting results are shown in Figure 3a, where the black curve is the experimental scattering data for dry S-SES(0), and the red curve is the fitted data. The domain spacing of dry S-SES membranes, d_{dry}, was calculated using $d_{dry} = 2\pi/q^*$, where q^* is the peak position obtained from the Lorentzian fits. Figure 3b shows d_{dry} as a function of ϕ_v. For dry S-SES membranes, d_{dry} ranged from 38.6 nm to 42.1 nm. The full width at half maximum (FWHM) of the peaks as a function of ϕ_v is shown in Figure 3c.

FWHM for dry S-SES(30) (ϕ_v = 0.29) is unusually large compared to the rest of the membranes; the FWHM of the other membranes increased slightly with increasing ϕ_v.

The SAXS characterization was complemented by examining the STEM images of these membranes collected using a high angle annular dark field (HAADF) detector, shown in Figure 4. These samples were not stained. The contrast on the images reflects the atomic number of the atoms in the samples (*z*-contrast). In dry samples, the bright regions are the sulfur-containing PSS-rich domains, since sulfur is the heaviest atom in S-SES membranes. The dark regions are the PE-rich domains. The domain spacing measured by SAXS is indicated by the yellow scale bar on each image. We observe good agreement between STEM images and the SAXS results. S-SES(0), S-SES(10) and S-SES(20) all exhibited lamellar morphology. For brevity, we did not show the STEM image of S-SES(10). S-SES(40) showed a bicontinuous morphology (Figure 4d). The morphology of S-SES(30) is less well-defined (Figure 4c), as it is located at the cross-over from lamellar to bicontinuous morphology. We see regions with lamellar morphology similar to that of S-SES(20) and regions with bicontinuous morphology similar to that of S-SES(40). This explains the unusual change in d_{dry} and the unusually large FWHM of the SAXS profile of dry S-SES(30) (Figure 2).

SAXS results of hydrated S-SES membranes equilibrated in water are shown in Figure 5. We observed a strong secondary peak arising in all of S-SES membranes when they are immersed in water. The origin of this

secondary peak is due to a separate water-rich phase in the center of the PSS-rich domains when S-SES membranes are equilibrated with liquid water, as established in ref 26[26] where we showed consistency between the Fourier transform of the electron density distribution determined from electron micrographs and the SAXS profiles. We fitted the scattering profiles of hydrated S-SES membranes with Lorentzian functions, following the same procedure as the peak fitting of the dry S-SES membranes. Typical peak fitting results are shown in Figure 6a. The bottom red curves are fitted results for the primary peak (labeled as Peak 1) and the secondary peak (labeled as Peak 2). The top red curve in Figure 6a is the sum of Peak 1 and Peak 2 and it is overlaid on the experimental data for hydrated S-SES(0) (black curve).

The domain spacing of hydrated S-SES membranes, d_{wet}, was calculated using $d_{wet} = 2\pi/q_1$, where q_1 is the peak position of the primary peak obtained from the Lorentzian fit results of Peak 1. Hydrated domain spacing d_{wet} as a function of ϕ_v is plotted in Figure 6b. The FWHM of Peak 1 as a function of ϕ_v is shown in Figure 6c. At low ϕ_v values, FWHM was low: 0.033 nm^{-1} at $\phi_v = 0$ and 0.028 nm^{-1} at $\phi_v = 0.19$. At high ϕ_v values, FWHM increased to 0.056 nm^{-1} at $\phi_v = 0.29$ and 0.049 at $\phi_v = 0.39$. We also show q_2/q_1 as a function of ϕ_v in Figure 6d, where q_2 is the peak position of the Lorentzian function for Peak 2. At low ϕ_v values (0 – 0.19) wherein the samples are lamellar, q_2/q_1 is constant with a value of about 1.8. At higher

concentrations, q_2/q_1 decreases with increasing ϕ_v. This decrease is a characteristic of hydrated bicontinuous morphologies in our S-SES samples.

Cryo-STEM images of hydrated S-SES membranes are shown in Figure 7. The domain spacing measured by SAXS is indicated by the yellow scale bar on each image. Good agreement is again observed between STEM images and the SAXS results. Hydrated S-SES(0) and S-SES(20) exhibited a lamellar morphology (Figure 7a and 7b), similar to the morphology obtained in the dry state. We see three levels of intensity in the STEM images. This morphology has been thoroughly discussed in refs 26 and 30.[26, 30] The dark stripes representing the non-hydrated crystalline PE lamellae. Between two dark stripes are two bright stripes. They present the hydrated PSS chains in the form of a brush that emanates from the PE lamellae. Between two opposing hydrated PSS brushes is a single grey stripe, representing at water-rich channel (this channel is largely devoid of PSS chains). Hydrated S-SES(40) showed a bicontinuous morphology (Figure 4d). In this sample, the PSS-rich microphase swells to such an extent that it becomes the majority phase. The water-rich phase in S-SES(40) is not as clear as that in S-SES(0) and S-SES(20), but we do observe three levels of intensities on the micrograph: the brightest regions at the edge of hydrated PSS-domains, which are hydrated PSS brushes; the grey regions in the center of the hydrated PSS-domains are the water-rich phase; and the darkest regions are the PE-rich phase. Hydrated S-SES(30) is a transition between lamellar and bicontinuous morphology. Similar to S-SES(40), the water-rich phase in S-

SES(30) is less clear but we do observe three levels of intensities on the micrograph.

It is important to recognize that proof of a pure water channel in microphase separated systems is not trivial to obtain. In our lamellar samples (Figure 7a and 7b), the water channels can clearly be seen when the lamellae are orthogonal to the sample plane, as the entire channel contributes constructively to the contrast between the channel and the hydrated PSS brush in the image. Such constructive enhancement of contrast does not occur in bicontinuous morphologies. We use the SAXS data from hydrated SES(30) and SES(40) to conclude the presence of water channels in the bicontinuous morphologies (Figures 7c and 7d).

We conducted cryogenic transmission electron tomography experiments on S-SES(40), in both dry and hydrated states to further characterize the bicontinuous morphologies in these systems. Figure 8a shows tomogram slices of the dry S-SES(40) sample. The tomogram tilt series were collected on a Gatan K2 camera with a zero-loss energy filter. The more electron dense PSS-rich phase appears dark in the micrograph and PE-rich phase is the bright regions. Note that the contrast is the opposite to STEM images in Figure 4 and 7 as the STEM images were dark field images and the tomogram series were bright field images. The tomogram was segmented to identify the PSS-rich phase and the results are shown in Figure 8c; the PSS-rich microphase is colored purple. The tortuous bicontinuous microphases are clearly seen in the tomography images. Similarly, hydrated

S-SES(40) also present a bicontinuous morphology, shown in Figure 9b and d. We cannot see the water-rich phase in the tomograms due to the lack of contrast as discussed above. It is evident that the PSS domains swell considerably in the hydrated state.

In Figure 9a we show the overall nanodomain swelling of hydrated S-SES membranes by plotting d_{wet}/d_{dry} determined from SAXS as a function of ϕ_v (open squares). Swelling ($d_{wet}/d_{dry} > 1$) is observed in all cases. At low ϕ_v values (0 – 0.19), d_{wet}/d_{dry} is about 1.45. At high ϕ_v values (0.29 – 0.39), d_{wet}/d_{dry} is about 1.26. There is an abrupt change in d_{wet}/d_{dry} between $\phi_v = 0.19$ and $\phi_v = 0.29$. This coincides with the morphological cross-over from a lamellar morphology to a bicontinuous morphology. We compared d_{wet}/d_{dry} with the macroscopic swelling of the membranes, V_{wet}/V_{dry} where V_{dry} is bulk volume of dry S-SES membrane and V_{wet} the that of the hydrated membranes. The values of V_{dry} and V_{wet} are based on the water uptake values and the densities of each component of the membrane (PE: 0.97 g/cm^3, PSS: 1.11 g/cm^3, PS: 1.04 g/cm^3 and water: 1.0 g/cm^3). The nominal size of the samples, V_{wet}/V_{dry}, increases substantially with increasing ϕ_v, as shown in Figure 9a (solid circles). The overall nanodomain swelling, d_{wet}/d_{dry}, however, exhibits an entirely different dependence on ϕ_v (Figure 9a, open squares).

The overall nanodomain spacing obtained from SAXS represents the sum of the PSS domains and the PE domains. We thus carried out further

analysis of the STEM images in order to study the swelling of individual domain sizes. The domain size of PSS and PE of dry as well as that of hydrated S-SES(0), S-SES(10) and S-SES(20) membranes were obtained through line analysis of the images. For S-SES(40), areal analysis was performed. For irregularly shaped S-SES(30), a combination of line (lamellar region) and areal analysis (bicontinuous region) was performed. In Table 2, we summarize the changes in the dimension of the hydrophobic (PE) and hydrophilic (PSS) domains in our samples induced by hydration. The PE domains shrink upon hydration; $d_{PE,wet}/d_{PE,dry}$ ranges from 0.67 to 0.84. In contrast, the PSS domains swell upon hydration, $d_{PSS,wet\text{-}total}/ d_{PSS,dry}$ ranges from 2.0 to 2.6. In addition, the PSS channels contain a water-rich channel in the middle that is 12-18 nm wide and it occupies 30-40% of the hydrated PSS microphase. The overall domain sizes determined by STEM and SAXS are in qualitative agreement (the average deviation between overall domain spacings determined by SAXS and STEM was 5 %).

Table 2. Individual domain spacing of S-SES membranes from STEM images

	S-SES(0)	**S-SES(10)**	**S-SES(20)**	**S-SES(30)**	**S-SES(40)**
$d_{PE,dry}$ **(nm)**	19.3 ± 2.5	20.9 ± 5.0	20.5 ± 2.4	18.2 ± 1.6	24.8 ± 3.2
$d_{PE,wet}$ **(nm)**	15.2 ± 2.8	15.8 ± 3.0	13.7 ± 2.7	15.3 ± 3.6	19.3 ± 3.8
$d_{PE,wet}/d_{PE,dry}$	0.79	0.76	0.67	0.84	0.78
$d_{PSS,dry}$ **(nm)**	20.0 ± 2.8	17.7 ± 5.5	19.6 ± 2.0	17.9 ± 3.0	16.6 ± 2.4
$d_{PSS,wet\text{-}total}$ **(nm)**	45.8 ± 4.8	46.8 ± 3.6	45.9 ± 6.0	36.6 ± 5.2	40.3 ± 6.3

$d_{PSS,wet-total}/d_{PSS,dry}$	2.3	2.6	2.3	2.0	2.4
$d_{PSS,wet-water\ channel}$ (nm)	14.4 ± 3.9	14.3 ± 2.5	17.7 ± 5.4	12.0 ± 4.1	Not measured

The average PSS domain spacing change, $d_{PSS,wet}/d_{PSS,dry}$, and the average PE domain spacing change, $d_{PE,wet}/d_{PE,dry}$, as a function of ϕ_v is plotted in Figure 9b. PSS domain swelled by about 240% in all membranes. In all cases, the swollen PSS domains contain water channels. Conversely, the domain size of PE decreased slightly in all cases ($d_{PE,wet}/d_{PE,dry} \approx 0.8$). The STEM analysis results indicate that PSS domains in all the membranes exhibited similar level of swelling after immersing in liquid water. Our observations are very different from the well-studied case of swelling of uncharged polymers, wherein the overall domain size, d, is often expressed as a power-law: $d = k(1-\phi_s)^{\alpha}$ where ϕ_s is the solvent volume fraction, and k and α are system-dependent constants. For good non-selective solvents, α=0.17, while for selective solvents, α ranges between -2 and -3.[31-33]

Conclusions

In this work, we examined the swelling of a series of block copolymer electrolytes immersed in liquid water. We focused on the swelling (and deswelling) of individual domains due to exposure to water. The series was prepared by mixing varying amounts of a polystyrene homopolymer in a polystyrene-*b*-polyethylene-*b*-polystyrene, casting the mixture to obtain a membrane, extracting the homopolymer to obtain nanoscale voids, and

sulfonating the membrane. In the neat state, these sulfonated polystyrene-*b*-polyethylene-*b*-polystyrene (S-SES) membranes have the same chemical composition (differing only slightly in sulfonation levels) but they exhibited a crossover from lamellar to bicontinuous morphology with increasing void fraction. The water update is a strong function of void fraction, increasing by a factor of two in our experimental window. The overall swelling of the nanodomains, determined by SAXS, decreases slightly at the crossover due to the one-dimensional character of lamellae and the tree-dimensional character of the biocontinuous phase. The swelling of the hydrophilic PSS domains was independent of void fraction. The width of the swollen PSS domains increased by about 240% due to exposure to water. A water-rich channel (largely devoid of PSS chains) is obtained in the middle of the domains. Exposure to water results in a slight deswelling of the hydrophobic PE domains, decreasing by about 20% relative to their value in the dry state. These changes, determined by a combination of cryogenic scanning transmission electron microscopy, and cryogenic electron tomography, cannot be anticipated from changes in the overall domain spacing measured by SAXS and macroscopic water uptake measurements. Further work is required to establish the molecular underpinnings of our observations.

Acknowledgement

This work was primarily supported by the U.S. Department of Energy, Office of Science, Basic Energy Sciences, Materials Sciences and Engineering

Division under Contract No. DE-AC02-05-CH11231 within the Electron Microscopy of Soft Matter Program (KC11BN). SAXS experiments were performed at the Advanced Light Source (ALS), Beamline 11.0.1.2. STEM experiments were performed at the National Center for Electron Microscopy (NCEM), Molecular Foundry, Lawrence Berkeley National Laboratory. Electron tomography was performed with facilities supported by National Institutes of Health Grant No. GM051487.

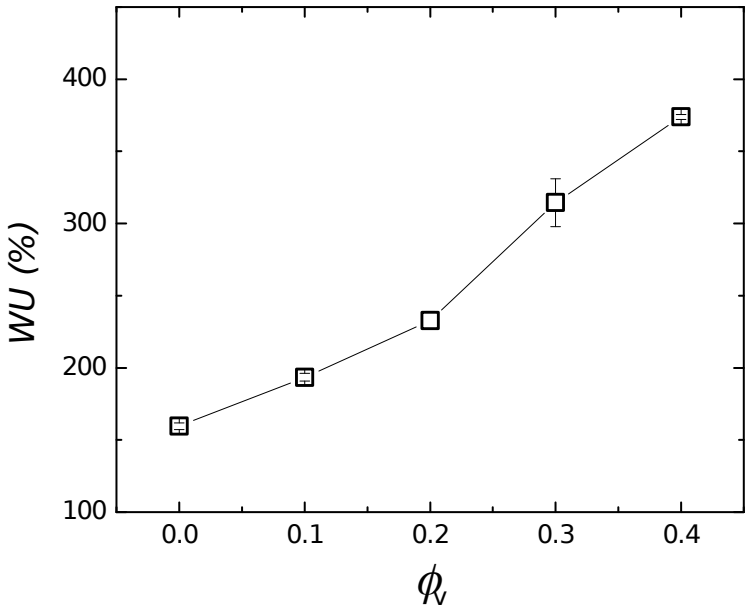

FIG 1. Water uptake, *WU*, as a function of ϕ_v.

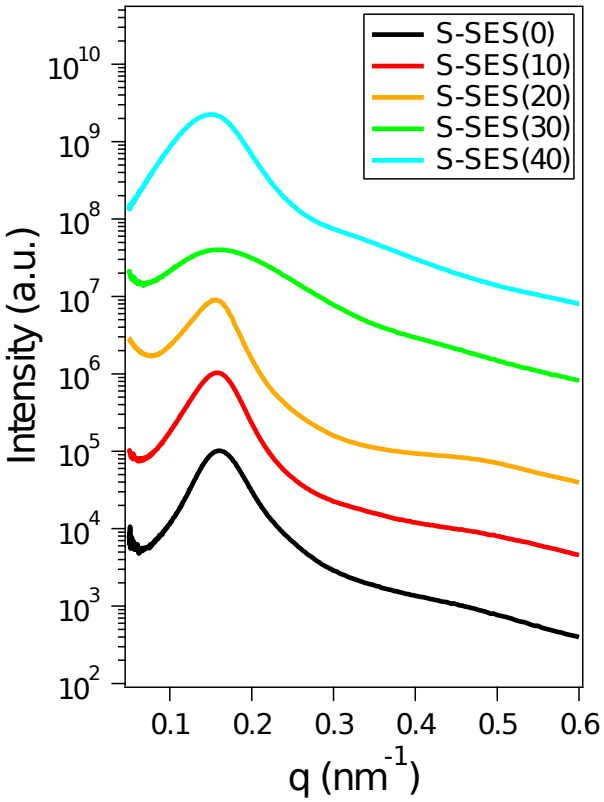

FIG 2. SAXS intensity as a function of the magnitude of the wave vector, q, of dry S-SES membranes. Profiles are vertically shifted for clarity.

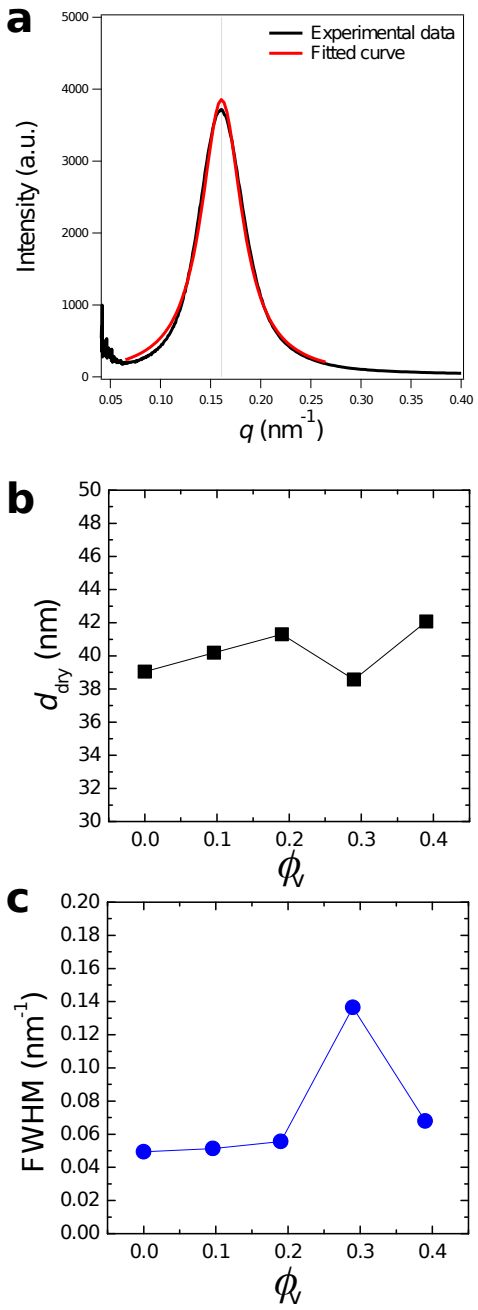

FIG 3. **a**, Peak fitting results of the SAXS profile of dry S-SES(0). **b**, domain spacing of the dry membranes, d_{dry}, as a function of ϕ_v. **c**, FWHM of the fitted SAXS peaks as a function of ϕ_v.

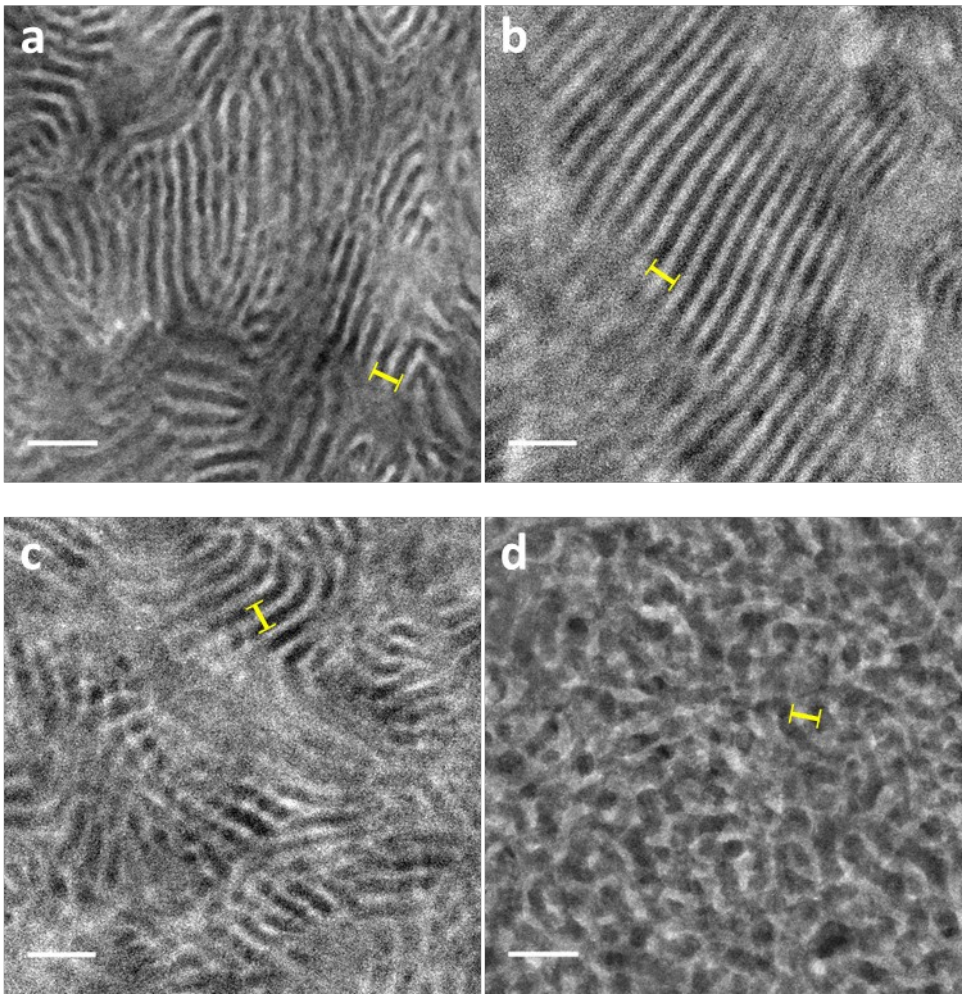

FIG 4. STEM images of dry S-SES membranes. **a**, S-SES(0), **b**, S-SES(20), **c**, S-SES(30) and **d**, S-SES(40). White scale bar on the bottom left represents 100 nm. Yellow scale bar represents domain spacing obtained by SAXS.

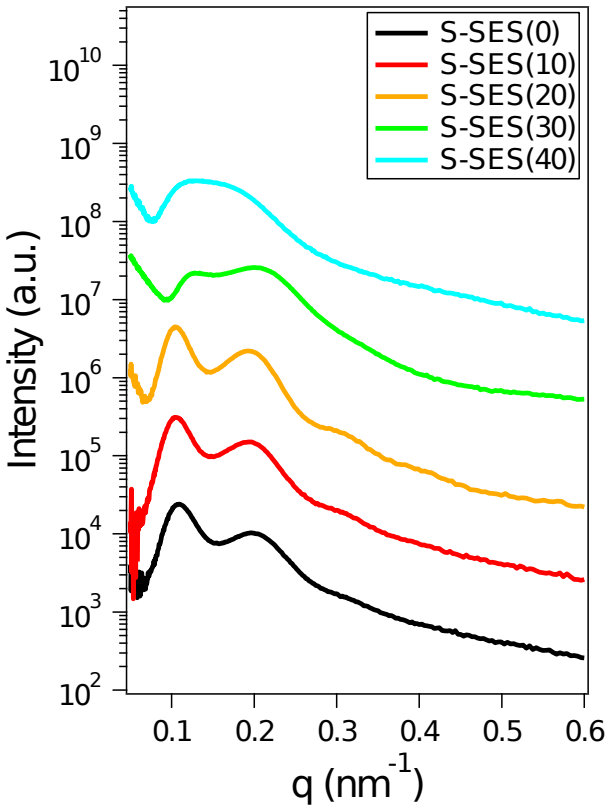

FIG 5. SAXS intensity as a function of q, of hydrated S-SES membranes. Profiles are vertically shifted for clarity.

F

I

G

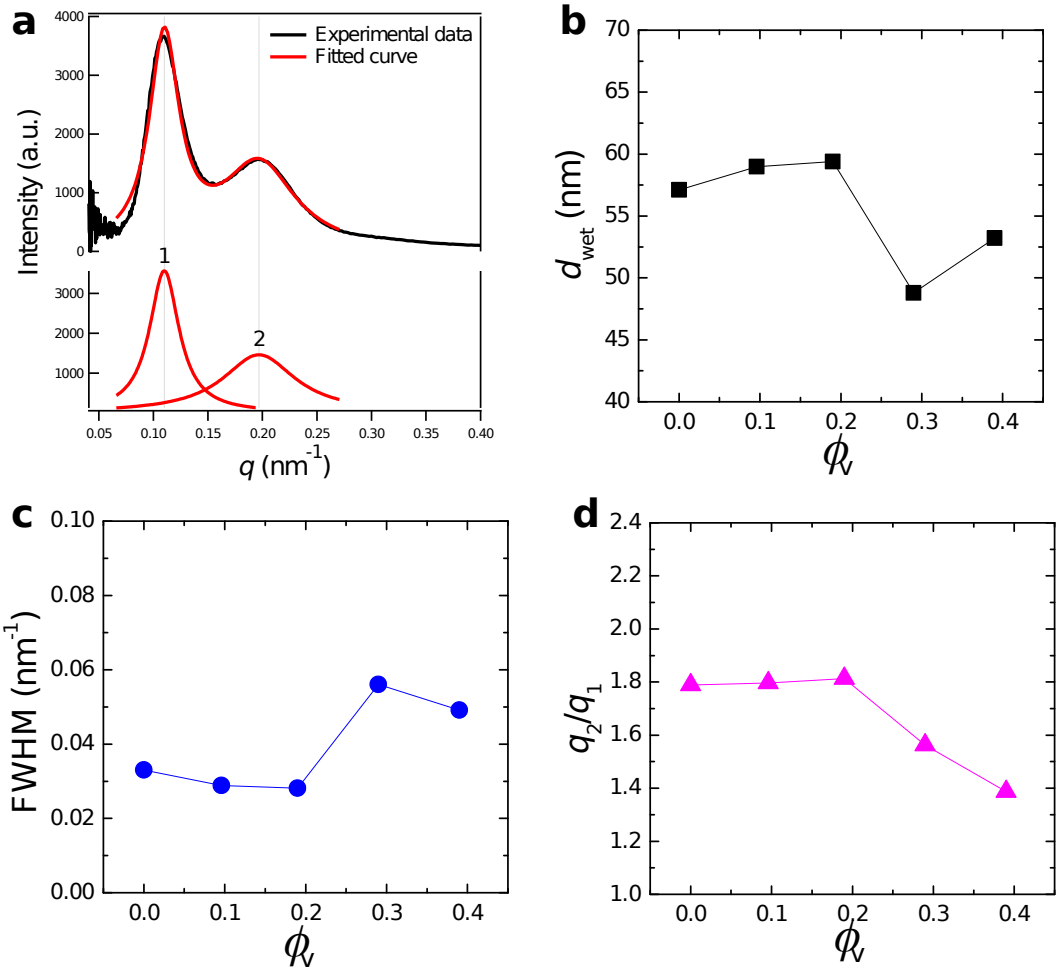

6. **a**, Peak fitting results of the SAXS profile of hydrated S-SES(0). The bottom red curves are fitted results for the primary peak (labeled as Peak 1) and the secondary peak (labeled as Peak 2). The top red curve is the sum of Peak 1 and Peak 2 and it is overlaid with experimental data for hydrated S-SES(0) (black curve) **b**, domain spacing of the hydrated membranes, d_{wet}, as a function of ϕ_v. **c**, FWHM of the fitted Peak 1 as a function of ϕ_v. **c**, q_2/q_1 as a function of ϕ_v, where q_1 is the fitted peak position of Peak 1 and q_2 is the fitted peak position of Peak 2.

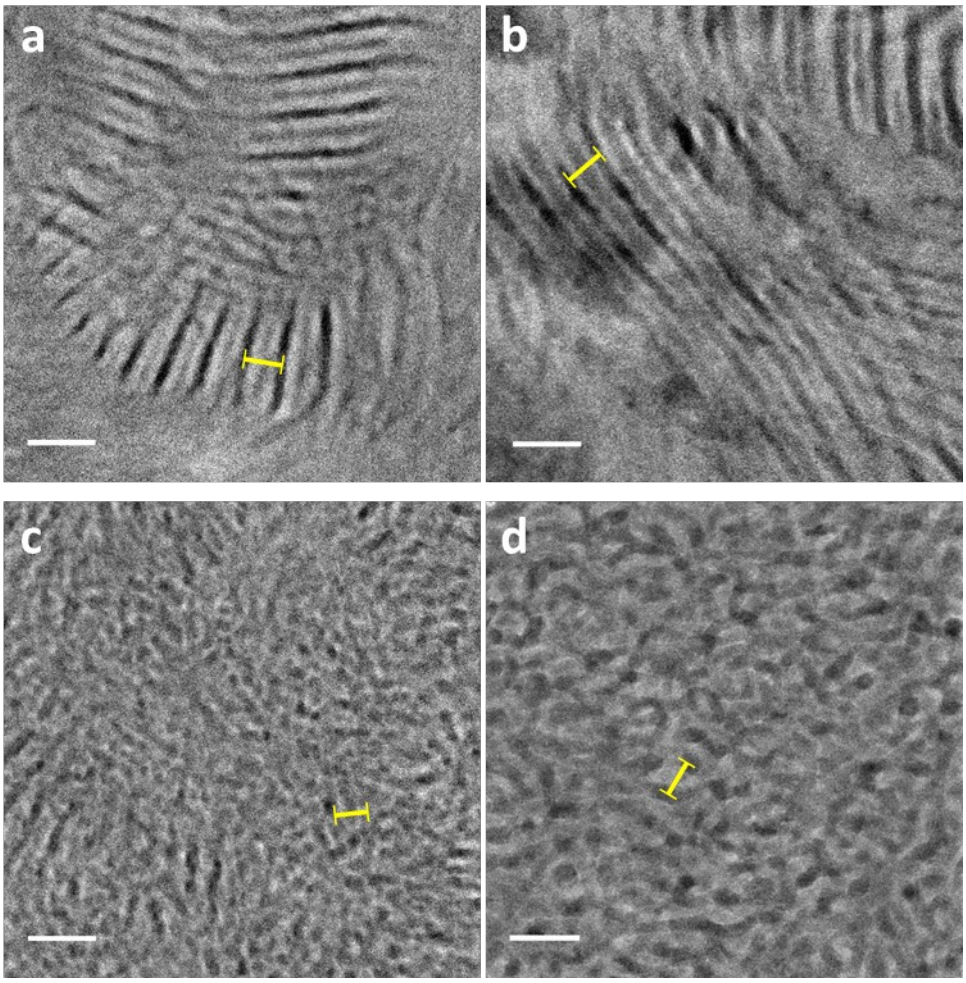

FIG 7. Cryo-STEM images of hydrated S-SES membranes. **a**, S-SES(0), **b**, S-SES(20), **c**, S-SES(30) and **d**, S-SES(40). White scale bar on the bottom left represents 100 nm. Yellow scale bar represents domain spacing obtained by SAXS.

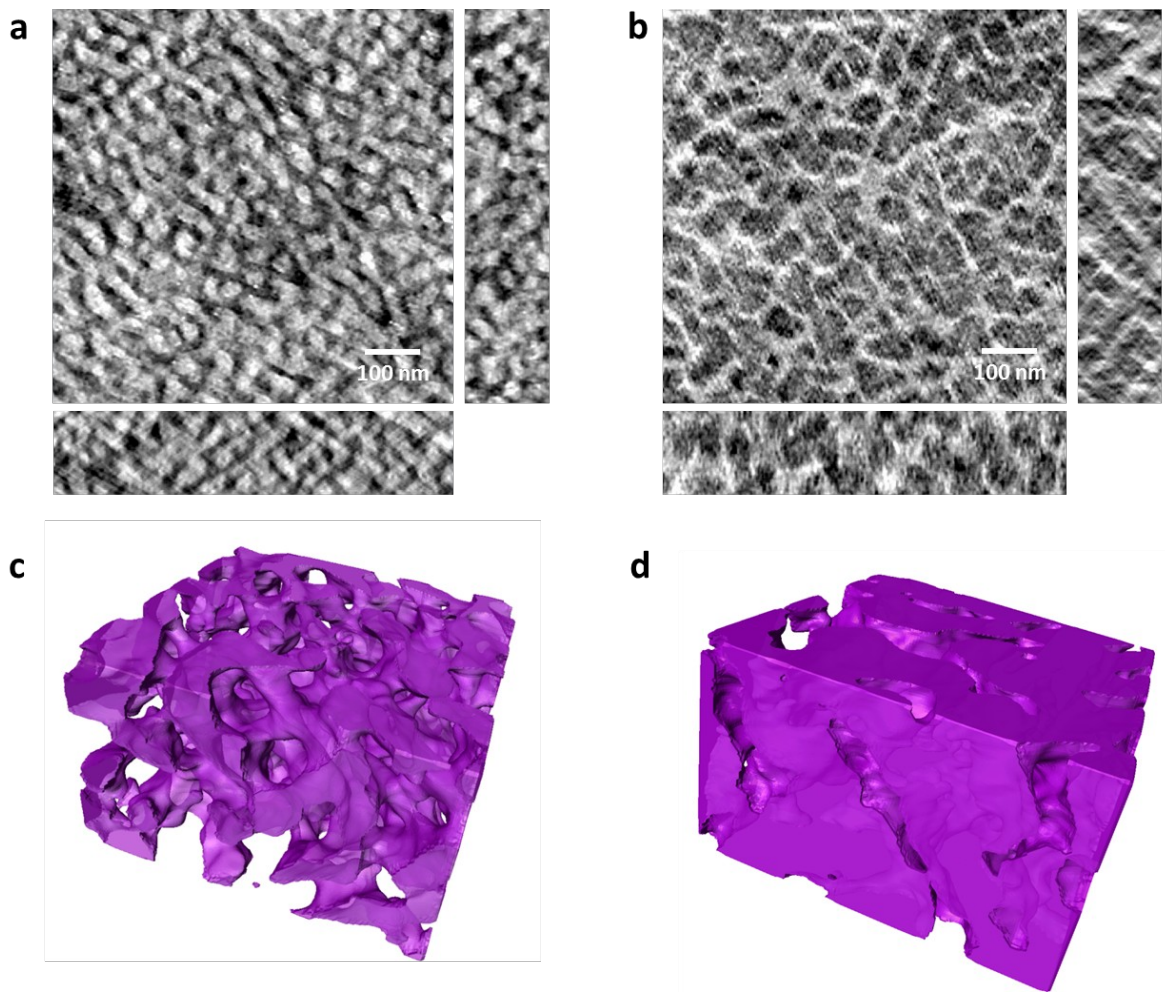

FIG 8. **a**, tomography slices of dry S-SES(40) in xy, yz, and xz directions. **b**, tomography slices of hydrated S-SES(40) in xy, yz, and xz directions. **c**, segmented dry S-SES(40), where purple colored segments represent dry PSS-rich phase. **d**, segmented hydrated S-SES(40), where purple colored segments represent hydrated PSS-rich phase.

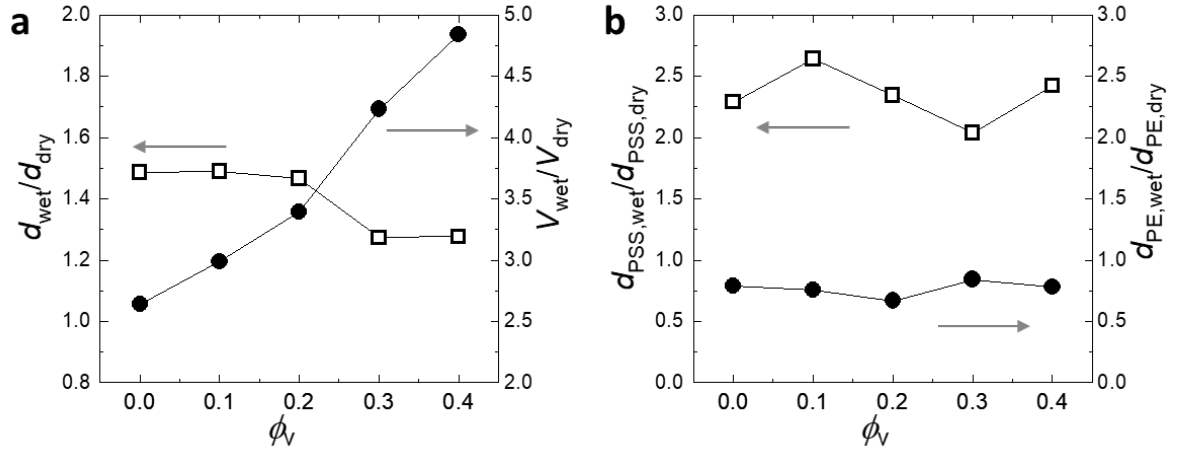

FIG 9. a, Nanodomain swelling d_{wet}/d_{dry} and macroscopic swelling V_{wet}/V_{dry} as a function of ϕ_v in S-SES membranes. b, Individual microphase spacing change $d_{PSS,wet}/d_{PSS,dry}$ and $d_{PE,wet}/d_{PE,dry}$ as a function of ϕ_v in S-SES membranes.

References

1. C. H. Park, C. H. Lee, M. D. Guiver, Y. M. Lee, Prog. Polym. Sci. **36**, 1443 (2011).
2. K. M. Beers, N. P. Balsara, ACS Macro Lett. **1**, 1155 (2012).
3. Q. H. Liu, G. M. Grim, A. B. Papandrew, A. Turhan, T. A. Zawodzinski, M. M. Mench, J. Electrochem. Soc. **159**, A1246 (2012).
4. B. R. Chalamala, T. Soundappan, G. R. Fisher, M. R. Anstey, V. V. Viswanathan, M. L. Perry, P. IEEE **102**, 976 (2014).
5. R. Bouchet, S. Maria, R. Meziane, A. Aboulaich, L. Lienafa, J. P. Bonnet, T. N. T. Phan, D. Bertin, D. Gigmes, D. Devaux, R. Denoyel, M. Armand, Nat. Mater. **12**, 452 (2013).
6. R. Yuan, A. A. Teran, I, Gurevitch, S. A. Mullin, N. S. Wanakule, N. P. Balsara, Macromolecules **46**, 914 (2013).
7. M. A. Hickner, Mater. Today **13**, 34 (2010).
8. J. J. Krol, M. Wessling, H. Strathmann, J Membrane Sci **162**, 145(1999).
9. T. A. Zawodzinski, M. Neeman, L. O. Sillerud, S. Gottesfeld, J. Phys. Chem. **95**, 6040 (1991).
10. T. A. Zawodzinski, C. Derouin, S. Radzinski, R. J. Sherman, V. T. Smith, T. E. Springer, S. Gottesfeld, J. Electrochem. Soc. **140**, 1041 (1993).
11. T. A. Zawodzinski, J. Davey, J. Valerio, S. Gottesfeld, Electrochim. Acta **40**, 297 (1995).
12. Y. A. Elabd, E. Napadensky, C. W. Walker, K. I. Winey, Macromolecules **39**, 399 (2005).
13. Y. A. Elabd, C. W. Walker, F. L. Beyer, J Membrane Sci **231**, 181 (2004).
14. S. Y. Kim, S. Kim, M. J. Park, Nat Commun **1**, 88 (2010).
15. S. Y. Kim, E. Yoon, T. Joo, M. J. Park, Macromolecules **44**, 5289 (2011).
16. T. J. Peckham, J. Schmeisser, M. Rodgers, S. Holdcroft, J. Mater. Chem. **17**, 3255 (2007).
17. G. Gebel, P. Aldebert, M. Pineri, Polymer **34**, 333 (1993).
18. G. Gebel, Polymer **41**, 5829 (2000).
19. M. A. Modestino, D. K. Paul, S. Dishari, S. A. Petrina, F. I. Allen, M. A. Hickner, K. Karan, R. A. Segalman, A. Z. Weber, Macromolecules **46**, 867 (2013).
20. Y. A. Elabd, M. A. Hickner, Macromolecules **44**, 1 (2010).
21. M. J. Park, K. H. Downing, A. Jackson, E. D. Gomez, A. M. Minor, D. Cookson, A. Z. Weber, N. P. Balsara, Nano Lett. **7**, 3547 (2007).
22. A. Arceo, P. F. Green, J Phys Chem B **109**, 6958 (2005).
23. K. J. Hanley, T. P. Lodge, C. I. Huang, Macromolecules **33**, 5918 (2000).
24. M. J. Park, N. P. Balsara, Macromolecules **41**, 3678 (2008).
25. M. J. Park, A. J. Nedoma, P. L. Geissler, N. P. Balsara, A. Jackson, D. Cookson, Macromolecules **41**, 2271 (2008)
26. X. C. Chen, D. T. Wong, S. Yakovlev, K. M. Beers, K. H. Downing, N. P. Balsara, Nano Lett. **14**, 4058 (2014).
27. X. C. Chen, J. B. Kortright, N. P. Balsara, Macromolecules **48**, 5648 (2015).

28. X. Wang, K. M. Beers, J. B. Kerr, N. P. Balsara, Soft Matter **7**, 4446 (2011).
29. K. M. Beers, D. T. Wong, A. J. Jackson, X. Wang, J. A. Pople, A. Hexemer, N. P. Balsara, N. P. Macromolecules, **47**, 4330 (2014).
30. X. C. Chen, H. J. Oh, J. F. Yu, J. K. Yang, N. Petzetakis, A. S. Patel, S. W. Hetts, N. P. Balsara, ACS Macro Lett. **5**, 936 (2016).
31. N. P. Balsara, C. E. Eastman, M. D. Foster, T. P. Lodge, M. Tirrell, Makromol Chem-M. Symp. **45**, 213 (1991).
32. M. D. Whitmore, J. Noolandi, J. Chem. Phys. **93**, 2946 (1990).
33. J. M. Virgili, A. Hexemer, J. A. Pople, N. P. Balsara, R. A. Segalman Macromolecules **42**, 4604 (2009).